Direct and Inverse "Cascade" during Fragmentation of a Liquid Metal Jet into Water

Nicolas Rimbert, Miloud Hadj-Achour, Gagan Kewalramani, Bowen Ji, Alexandre Labergue, Michel Gradeck, Renaud Meignen

Direct and Inverse "Cascade" during Fragmentation of a Liquid Metal Jet into Water

Nicolas Rimbert,* Miloud Hadj-Achour, Gagan Kewalramani, Bowen Ji, Alexandre Labergue, and Michel Gradeck
LEMTA, CNRS Université de Lorraine, Vandœuvre-lès-Nancy, 54518, France

Renaud Meignen
Institut de Radioprotection et de Sûreté Nucléaire (IRSN) Saint Paul Lez Durance, 13115, France
(Dated: December 6, 2021)

This paper presents experimental results on the fragmentation of a low meting point liquid metallic alloy jet into water. The liquid is Field's metal whose melting point is 62°C. Data are obtained using high-speed camera acquisition and the solidified particles are sieved, a size Probability Distribution Function (PDF) is obtained from their mass distribution. These results are compared to separate data acquisitions obtained using a phase Doppler anemometer (PDA used in reflexion regime). Injection diameter range from 1 mm to 5 mm and injection velocity from 2.28 m/s to 4.97 m/s resulting in a (carrier phase) Weber number ranging from 15 to 281 and a (carrier) Reynolds number ranging from 2500 to 24000. The conclusion is that for these intermediate Weber and Reynolds numbers, the size of the droplets can mainly be related to a cascading instability mechanism: first Entov & Yarin bending instability which is then closely followed by a Rayleigh-Taylor instability. Moreover, the Mass Probability Distribution Function (PDF) can be approximated by a log-stable laws whose parameters can be computed using wavelengths stemming from the cascade of instability scenario. However, the smallest droplets or ligaments can eventually reach the turbulent dissipation length-scales where they are re-agglomerated by the turbulent movements. This results now in a Number PDF that also follows a log-stable law. For this part of the distribution, it is also possible to compute the parameters of the distribution without using any fitting parameter, by estimating the different turbulent scales. In this setting, atomization looks like a competition between a direct "cascade" of fragmentation instability and an inverse "cascade" of turbulent re-agglomeration

PACS numbers: May be entered using the `\pacs{#1}` command.

I. INTRODUCTION

Atomization and Sprays have a wide range of applications. The present paper is dedicated to the study of liquid-liquid fragmentation with high density ratio. Its main application is the understanding of severe nuclear accident where molten corium can interact with surrounding water. The residual heat of almost 3000°C hot Corium makes this interaction mostly water vapour/corium; nevertheless, the use of low(er)-melting point alloy is a classical way of recovering both the high-density density ratio and the high surface tension of the melt while working in simpler and safer conditions [1–4]. The present study goes one step further in the simplification as overheating of the molten metal is low enough so that no vapour is ever produced. This allows for the combined use of optical methods (shadowgraphy, Phase Doppler Anemometer...*etc.*) and traditional sieving methods [5]. The strategy is to use these more accurate and non-intrusive optical diagnostics to build more precise models that could eventually be used on the real case.

As far as atomization modelling is concerned, recent advances on the modelling of this topic, mostly concerns the influence of ligament intermediate in the fragmentation process [6], though not really new (see [7] for instance). The main result of the authors, here, is that it leads to a Gamma distribution of the daughter droplets. However, no leads to how-to compute parameters of the Gamma distribution has been found in the general case up to now. This seems to compete with Kolmogorov analysis [8] leading to log-normal distribution which has been recently modernized [9–12]. In this case also, the computation of the parameters in the general case is difficult though some models do exist. Last, competition between classical instabilities such as Rayleigh-Taylor instability (often associated to bag-breakup) or Kelvin-Helmholtz instabilities (often associated to boundary layer stripping) is known to be fundamental, at least near the instability threshold. This led to quite intricate models such as [13] which are still used nowadays in commercial Computer Fluid Dynamics codes. There are however a large quantity of other instability models that pertain to this field (see for instance [14] for a partial review).

In the wake of these works, Rimbert & Séro-Guillaume [11], developed an extension of Kolmogorov's work to log-stable law and applied it successfully to high-Weber number (third party) spray Mass Probability Distribution Function (PDF). These laws are generalizations of log-normal laws and are sometimes known as universal multifractals [15, 16]. However, in this first work, the parameter were fitted and no explanation about their value was given. Building on Kida's work [17, 18], Rimbert [19] gives a possible explanation (self-avoiding vortex tangles

* nicolas.rimbert@univ-lorraine.fr

related to angular momentum conservation) for the importance of log-stable law in the modelling of fine-scale structure of turbulence, but most importantly, also gives a way to compute several parameters of the dissipation distribution. This allows Rimbert & Castanet [20] to propose a model to compute the fine-size droplet PDF in a fan-spray based on the following assumptions: (i) instabilities do govern the triggering of the fragmentation process and the size of the largest fragments; (ii) formation of the final droplet is mediated by transitory ligament-shaped blobs of liquids; (iii) final size of the droplet is governed by interaction of the ligaments with surrounding turbulence. This results in a fine-size droplet Number PDF that can also be approximated by a log-stable law. There is therefore a discrepancy between these two approaches, [11] presents a self-similar Mass PDF cascading mechanism valid for high Weber number while [20] presents a turbulent re-agglomeration mechanism of small ligaments valid for intermediate Weber number and leading to a Number PDF.

The purpose of present work is to show how both these previous models allows for the computation of the droplet PDF in present liquid-liquid case. The large size PDF has been found to be mainly driven by large scale instabilities in a successive manner: first Entov & Yarin bending instability [21] and then more classically Rayleigh-Taylor instability. However, small scales, sensitive to turbulent agitation, seems also governed by a re-agglomeration mechanism. It will also tentatively show how to compute all the relevant parameters of the distributions.

II. EXPERIMENTAL SET-UP

The experimental set-up is a modification of the drop-on-demand set-up used in Hadj-Achour *et al.* [5], himself derived from Amirzadeh *et al.* [22]. The liquid metal injector is represented on figures 1 and 2. It uses Field's metal, a eutectic alloy of Tin, Bismuth and Indium, whose melting temperature is 62°C. The temperature of the melt (85°C) is kept by a double-boiler ("bain-marie") technique. The measured density of Field's metal is $7994 kg/m^3$, its viscosity is approximately 10 mPa.s (and very sensitive to oxidation when tested in a Couette viscosimeter) and its surface tension is 0.41 N/m when compared to water (it has been measured by the ADSA technique [5]).

The GaLaD (for "Goutte à La Demande" *i.e.* Drop-On-Demand) experimental setup (*cf.* figure 1) has been modified to include an electro-magnet (*cf.* figure 2) that allows for the opening of the stem-valve for a longer time thereby generating a jet (henceforth named JaLaD for "Jet à La Demande" *i.e.* Jet-On-Demand). The velocity of the jet is controlled by varying the pressure of the Nitrogen gas-supply. The new set-up as well as the set-up of the Dantec Phase Doppler Anemometer (PDA) is shown on figure 3.

The size of the water pool is 50cm × 50cm × 40cm and is

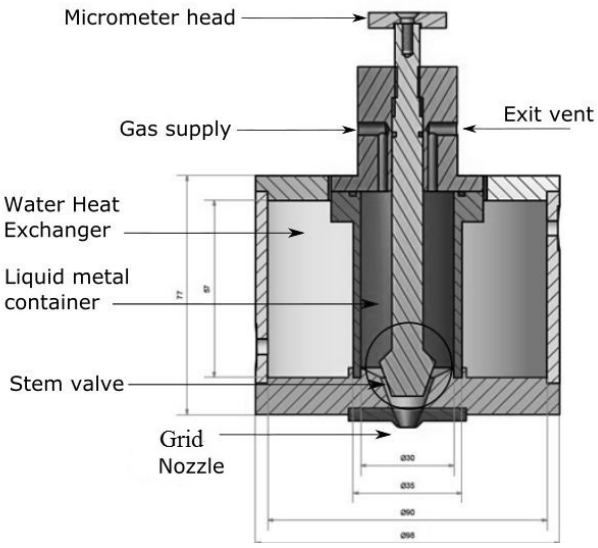

Figure 1. GaLaD experimental Set-up.

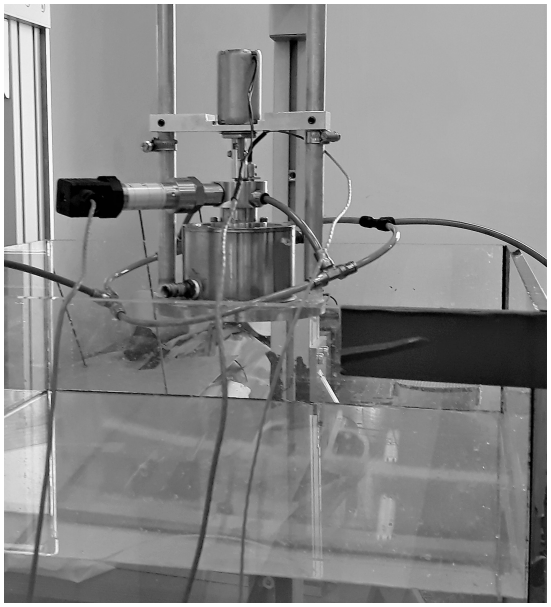

Figure 2. JaLaD experimental Set-up.

heated to 40°C. This choice stems from the initial liquid metal temperature set to 85 °C. To limit solidification impact during fragmentation, the pool temperature has been increased from ambient temperature to the limit where droplets were still liquid when they touched the bottom (50 °C). Therefore a lower value, of 40 °C, has been used for the pool temperature in most experiments to ensure that the fragments do not coalesce on the bottom (this value is actually limited by the height (40cm) of the pool as using a deeper pool would allow for a higher bath temperature). This corresponds to a contact temperature T_C of 75 °C, obtained by the following equation

(neglecting convection),

$$T_C = \frac{E_L T_L + E_C T_C}{E_L + E_C} \tag{1}$$

where E_L and E_C are respectively the thermal effusivity ($\sqrt{\lambda \rho C_p}$) of the Field's metal liquid droplet and ambient carrying water, T_C is the ambient carrying water pool temperature and T_L is the Field's metal liquid droplet temperature. Therefore it can be assumed that the jet disintegrates in the water but that the droplets solidify before they hit the bottom of the vessel where they will be eventually collected to be sieved.

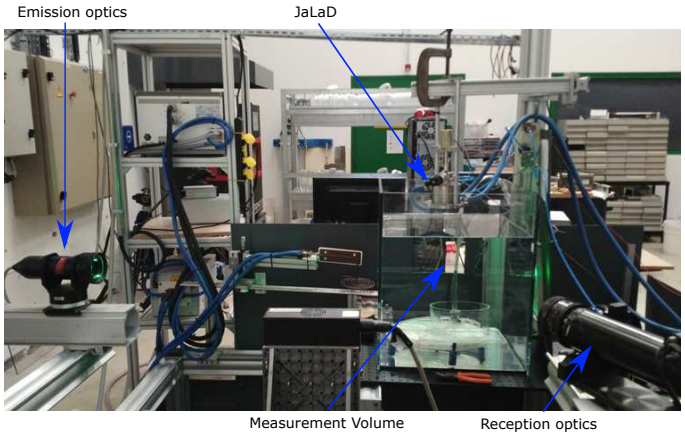

Figure 3. JaLaD experimental set-up for liquid metal jet into water.

As mentioned, three measurement techniques are used to study the jet disintegration. The first technique is high speed shadowgraphy. Imaging is obtained thanks to a LED back lighting (PRIOLITE LED 400 equivalent to 400W halogen light) and a phantom V701 high speed camera. The second is a Dantec PDA system whose configuration is given on table III. The third system is the simpler: it consists in a Retsch vibratory sieve shaker AS 200 which is used to separate the fragments according to their size. Each bin is thereafter weighted and the results recorder (in table II).

A. Non dimensional numbers

The four non dimensional parameters governing the hydrodynamics of the fragmentation are: the (carrier) Weber number We, the Ohnesorge number Oh,

$$We = We_C = \frac{\rho_C U_0^2 D_0}{\gamma}, \qquad Oh = \frac{\mu_L}{\sqrt{D_0 \rho_L \gamma}}, \tag{2}$$

the density ratio ρ_R and the viscosity ratio μ_R,

$$\rho_R = \frac{\rho_L}{\rho_C}, \qquad \mu_R = \frac{\mu_L}{\mu_C} \tag{3}$$

where ρ is the density, μ is the dynamic viscosity, γ is the surface tension, D_0 is the jet nozzle diameter and U_0 the jet initial velocity; subscript C indicates the property of the carrier phase (water) while subscript L indicates the property of the liquid metal phase (Field's metal). In the present case, the Weber number is the main hydrodynamic parameter.

Other important non dimensional parameters can be deduced from the four above, they are: the Reynolds numbers (for the carrier and the liquid)

$$Re_C = \frac{\rho_C U_0 D_0}{\mu_C}, \qquad Re_L = \frac{\rho_L U_0 D_0}{\mu_L} \tag{4}$$

and the liquid Weber number

$$We_L = \frac{\rho_L U_0^2 D_0}{\gamma}. \tag{5}$$

Note that $Oh = \sqrt{We_L}/Re_L$.

B. High Speed Shadowgraphy

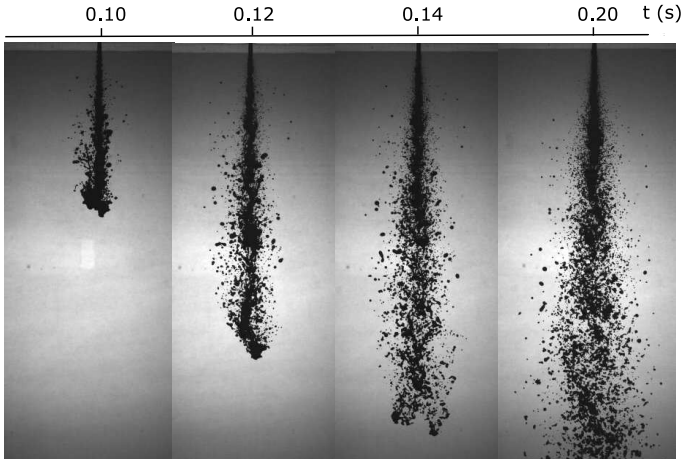

Figure 4. Shadowgraph images for D2P6 experiment.

Figure 4 shows a sample shadowgraph. The pressure is imposed in the gas tank and measure of the tip penetration speed gives us an estimate of the jet velocity U_0. Table I indicate the four different experimental conditions for the combined shadowgraph/sieving experiments.

Test	D_0	Pressure	U_0 (m/s)	We	Oh	SMD/D_0
D2P6	2 mm	6 bar	2.3	26.45		0.47
D2P10	2 mm	10 bar	2.8	39.2		0.29
D5P6	5 mm	6 bar	4.3	225		0.15
D5P10	5 mm	10 bar	4.8	281		0.11

Table I. Experimental conditions for the high-speed shadowgraphy and the sieving experiments.

We	20 µm	50 µm	100 µm	500 µm	1 mm	2 mm	Total
26.45	0.3 g	0.9 g	10.9 g	34.7 g	60.7 g	13.4 g	120.4 g
39.2	0.6 g	1.2 g	24.7 g	59.2 g	23.9 g	45.8 g	132.9 g
225	0.4 g	1.7 g	15.5 g	23.2 g	60.7 g	30.6 g	132.1 g
281	1.1 g	2.4 g	19.2 g	33.0 g	57.3 g	11.6 g	124.6 g

Table II. Mass measurements by sieving. Note that the 100 µm sieve corresponds approximately to the resolution of the high-speed camera

C. Sieving Results

Table II indicate the resulting of the sieving of the solidified fragments for four separate cases (summarized by their Weber number) and the corresponding Mass PDF is given on figure 5 (Note that it is the Mass PDF for the logarithm of the diameter $\frac{1}{M_{tot}}\frac{dM}{dlog_{10}(D)}$ that is represented).

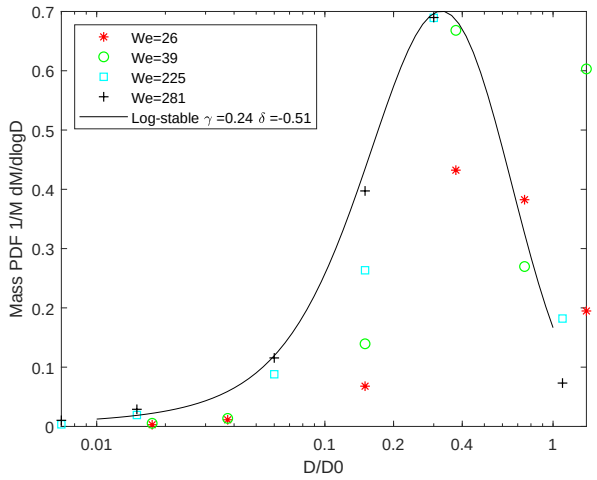

Figure 5. Mass Distribution

The values of Sauter Mean Diameter (SMD) given in table I are computed from table II using equations (6).

$$SMD = \frac{1}{\sum_{i=0}^{N_s} x_i/\bar{D}_i} \tag{6}$$

where x_i is the mass fraction of sieve number i and $\bar{D}_i = \frac{D_i+D_{i+1}}{2}$ is the average bin sieve diameter and N_s the number of sieves used. Note that for the largest (2mm) sieve, the $i+1^{th}$ sieve size has been set to $1.8\times D_0$ to account for droplets eventually generated by Rayleigh-Plateau instability. This has low impact on the SMD which gives more weight to the small droplets however. Figure 6 shows the evolution of SMD/D_0 ratio with Weber number. There appears to be a scaling

$$\frac{SMD}{D_0} \propto We^{-1/2} \tag{7}$$

This suggests that Rayleigh-Taylor instability may have its part to play in the present fragmentation mechanism. This is, however, left to next section.

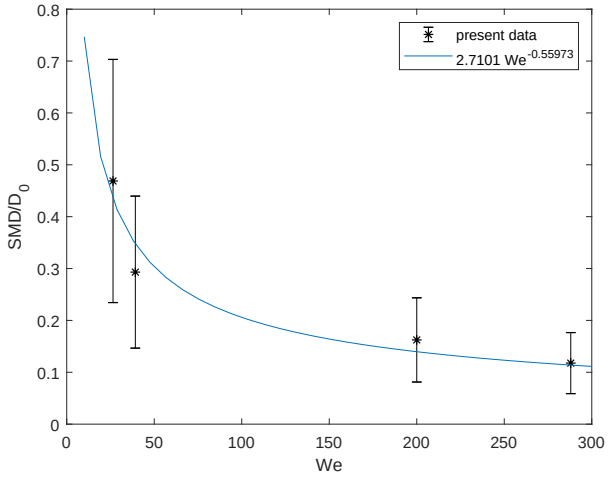

Figure 6. Sauter Mean Diameter as a function of Weber number

As in [5], equation (8)

$$C = \frac{1}{12}\frac{\rho_C}{\rho_L}\frac{D_0}{SMD}\frac{1}{We} \tag{8}$$

gives an estimate of the ratio between surface energy created during fragmentation to the kinetic energy of the spray. This ratio is given in percentage on figure 7 and is quite low, showing that powder production would need a lot of energy in this setup.

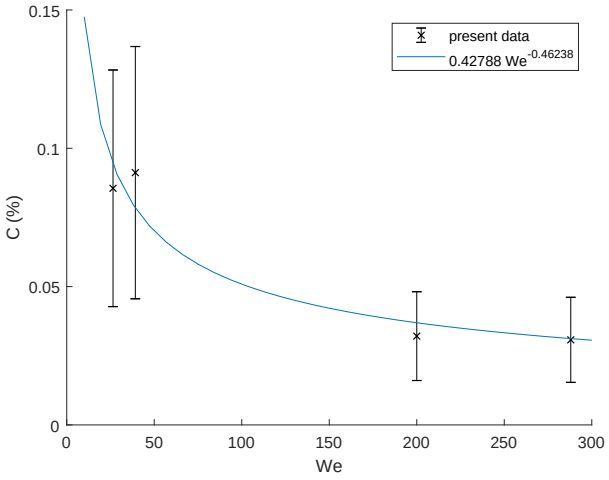

Figure 7. Kinetic to surface energy conversion ratio C as a function of Weber number

D. PDA Measurements

In order to study the small scale dynamics, we decided to use a Phase Doppler Anemometer that allows for the measurement of the joint size-velocity distribution. The number of bins in the PDF can be selected arbitrarily and we should have therefore a more precise determination of the shape of the PDF. However as it is based on droplet counting, this leads now to a Number PDF.

Parameter	Value
Green laser wavelength	514.5 (nm)
Blue laser wavelength	488 (nm)
Laser Beam Waist Radii	1.35 (mm)
Distance between separated laser beams	60 (mm)
Emission focal length	1200 (mm)
Reception focal length	500 (mm)
Observation angle	80°
Measurement angle (between beams)	0.05°
Green measurement volume	23.3mm × 0.58mm
Blue measurement volume	22.1mm × 0.55mm

Table III. Configuration of the Dantec PDA system.

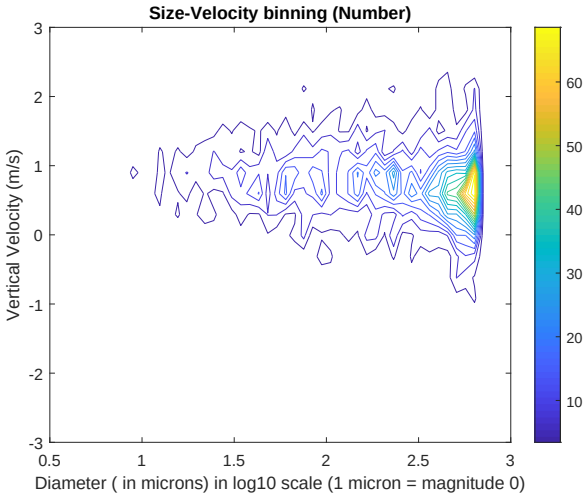

Figure 8. Size - Vertical Velocity measurements obtained from the PDA analysis. Measurement point is located 10cm below the injector, 1cm slightly off axis.

Due to the opacity of Field's metal, the PDA system was set in reflection mode. Unfortunately, it was not possible to use the 2mm and 5mm nozzle quantitatively in the PDA case, as they resulted in too short jets. Actually as JaLaD experiment is a converted drop-on-demand apparatus, it can only contain roughly 120g of liquid metal. Therefore, it empties quite quickly and a 1 mm nozzle was needed for this special case to make the jet last longer. Also related to small size of the container and the impossibility to make long sample, the setting of all parameters of the PDA (*cf.* table III) was previously done using glass beads in order to simplify the process. Injection pressure was set to 6 bar. The results in an injection velocity close to 2.5 m/s and a jet Weber number close to 15 and a carrier Reynolds number equals to roughly 2500 (as stated we had to slow down the jet to increase the experiment duration and reach a representative sample size). Figure 8 shows the joint size - vertical velocity PDF that has been measured out of 10,000 droplets. The measurement point is located 10cm below the nozzle (*i.e.* $100D_0$) and 1cm off axis. It can therefore be supposed that all the atomization process has stopped when the droplets are caught in the measurement volume. It is interesting to see that all the droplets seem to have the same velocity (close to 1m/s, *cf.* figure 9) independently from their size when this happens. It can also be seen that the fluctuations around this average velocity are great and can be evaluated to be also of the order of 1 m/s (therefore generating 100% turbulence intensity as usual in turbulent jets).

As their vertical velocity seems to be constant and independent from their size, it is therefore possible to compute the marginal size PDF of the droplet independently from their velocity. This is what is done on figure 10. Note that the cut-off of the PDA related to the shape of the measurement volume can be evaluated to be around 565µm if taking the average of the green and blue bands (*cf.* table III. Note that $log_{10}(0.565) = -0.25$ if reported on figure 10) while the measurements can be estimated to be precise until 316µm ($log_{10}(0.316) = -0.5$).

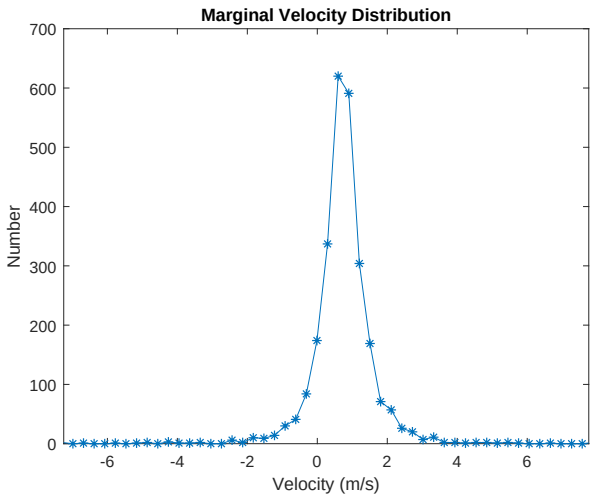

Figure 9. Number of droplets collected by the PDA according to the logarithm of their size. $We \approx 15$

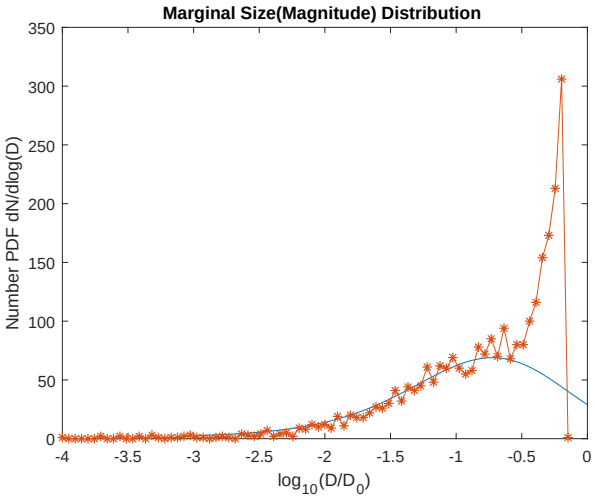

Figure 10. Number of droplets collected by the PDA according to the logarithm of their size. $We \approx 15$

III. MODELING OF THE EXPERIMENTAL RESULTS

A. "Direct Cascade" on Instability Scales

1. *Possible Instability Mechanisms*

We	λ_{EY}/D_0	λ_{KH}/D_0	λ_R/D_0	λ_T/D_0	η/D_0	$\epsilon(m^2/s^3)$
26	0.37	0.411	0.2	0.0351	1.8×10^{-3}	6083.5
39	0.35	0.277	0.135	0.0261	1.5×10^{-3}	10976
225	0.22	0.047	0.023	0.0055	4.48×10^{-4}	39753
281	0.21	0.038	0.018	0.0047	4.12×10^{-4}	55296

Table IV. Instability and turbulence characteristic length scales in the experiments

In this section, we propose to review some classical instability mechanisms and compare their most amplified wavelength to the size of the fragment hoping to be able to identify the underlying mechanisms. This is then extended to classical turbulence length scales. Therefore, the following characteristic length scale are computed: firstly, the wavelengths associated to the planar Kelvin-Helmholtz (*cf.* equation (9).

$$\lambda_{KH} = \frac{3\pi\gamma\left(\rho_C + \rho_L\right)}{U_0^2 \rho_C \rho_L} \tag{9}$$

Secondly, Rayleigh-Taylor instability most amplified wavelengths [23] are given by equation (10).

$$\lambda_{RT} = 2\pi\sqrt{\frac{3\gamma}{g\left(\rho_L - \rho_C\right)}} \tag{10}$$

where g is gravity acceleration. This results in a magnitude of $\lambda_{RT} \approx 2.6$cm which can be ruled out (except maybe at the tip of the jet (*cf.* figure 4 for t = 140 ms). Acceleration g could replaced by the jet deceleration but its value is not easy to determine precisely (being a second order time derivative of the jet position, it gives very noisy results) and is therefore not included here (but this idea will be used in the following).

Thirdly, in order to address quickly Sterling & Sleicher [24] or Lin & Kang [25] instability theory in cylindrical coordinates (that therefore involves Bessel functions, wind effect and the viscosity of the liquid), Reitz [26] developed an algebraic formula that interpolates efficiently Sterling & Sleicher results and allows for quick computations. It reads

$$\frac{\lambda_R}{D_0} = 18.04\frac{\left(1 + 0.45Oh^{0.5}\right)\left(1 + 0.4T^{0.7}\right)}{\left(1 + 0.87We_C^{1.67}\right)^{0.6}} \tag{11}$$

where

$$T = Oh\sqrt{We_C} \tag{12}$$

Results from Reitz, Sterling & Sleicher or Lin & Kang are, as expected, quite close and only values using Reitz method are actually reported here. Note that they predict wavelengths roughly half the value of planar Kelvin-Helmholtz instability as can be seen on table IV, showing that 2D axisymmetric correction has some importance.

Fourthly, Entov & Yarin [21] developed a slender jet analysis of the fragmentation mechanism where the jet is assumed to be a linear body submitted to a force and a torque generated by the surrounding fluid allowing for the bending of the jet. This leads to the following maximum amplified wave-number k_{EY}

$$k_{EY}D_0 = 2\left(\frac{2}{9}\frac{\rho_L D_0^2}{\mu_L^2}\left(\rho_C U_0^2 - \frac{2\gamma}{D_0}\right)\right)^{1/6} \tag{13}$$

Lastly, it is also interesting to compare these length scales with characteristic turbulent length scale. However the average turbulent kinetic energy dissipation rate ε is needed. It is estimated as usual [27] through equation (14)

$$\varepsilon \cong \frac{u'^3}{L_{\text{int}}}, \tag{14}$$

where u' represents the fluctuating velocity around the statistical average (using Reynolds decomposition). This allows for the computation of Taylor's characteristic turbulent length scale and Kolmogorov's length scale through equation (15) and (16).

$$\lambda_T = \sqrt{20\nu\frac{k}{\varepsilon}} \tag{15}$$

$$\eta \cong \left(\frac{\nu^3}{\varepsilon}\right)^{1/4} \tag{16}$$

In either eq. (14) or eq. (15), the kinetic energy of turbulence k is computed assuming that $u' \approx U$ which is usually assumed true for turbulent jets (and in agreement with the PDA results).

Table IV summarizes the results of such order of magnitude computations. It can be seen on figure 5, that most of the mass is located in the range [0.2, 0.5], showing that Entov & Yarin instability is the most likely candidate to explain the initial mass transfer along new scales in this fragmentation experiment. Actually, turbulence scales are so small that they do not seem to have an influence on the mass distribution at these Weber numbers.

2. Fitting the Mass Distribution

It can be seen on figure 5 a fit to the mass distribution with a log-stable law.

$$\frac{1}{M_{tot}}\frac{dM}{dlog_{10}(D)} \hookrightarrow p_\alpha(x;\beta,\sigma,\delta) \tag{17}$$

Let us recall that Lévy stable laws are defined from their Fourier transform [28]:

"A random variable X is said to have a stable distribution denoted $p_\alpha(x;\beta,\sigma,\delta)$ if there are real parameters $0 < \alpha \leq 2$, $0 < \sigma$, $-1 \leq \beta \leq 1$ and δ such that its characteristic function has the following form:

$$\hat{p}_\alpha(k;\beta,\sigma,\delta) = \exp\left(ik\delta - \sigma^\alpha |k|^\alpha \left[1 + i(sign(k))\beta\omega(|k|,\alpha)\right]\right) \tag{18}$$

where

$$\omega(|k|,\alpha) = \begin{cases} \tan(\alpha\pi/2) \text{if} \alpha \neq 1 \\ -(2/\pi)\log|k| \text{ if} \alpha = 1 \end{cases} \tag{19}$$

"

Simply put, the four parameters are respectively, α, the stability index governing the tail of the distribution, β the skewness parameter governing the symmetry of the law, δ the shift parameter governing the position of the maximum of the distribution and σ the scale parameter governing the width of the distribution. Gaussian laws are special cases of Lévy laws with parameter $\alpha = 2$, β being indifferent, δ being the average and σ the standard deviation. Except in the Gaussian case, Lévy laws are not square integrable, the standard deviation cannot usually be defined, hence the name scale parameter. Note that present modeling generalizes log-normal laws and not Gaussian laws as it is applied to the distribution of the logarithm of the diameter and not directly to the diameter. Rimbert [19] shows theoretically that the value that should be used to describe turbulence intermittencies are $\alpha = 1.7$, $\beta = -1$ (note that the distribution are said "totally skewed to the left" when $\beta = -1$). In order to keep the number of fitting parameters low, this value $\beta = -1$ has been kept as it is the only value that leads to finite moments of all positive orders. Moreover the value $\alpha = 1.7$ is related to angular momentum conservation and it has also been chosen to consider it set to this value. Therefore only the shift parameter and the scale parameters need to be fitted. The shift parameter has been set so that the maximum of the log-stable distribution coincides with the experimental PDF leading to the value $\delta = -0.55$ for the $We = 281$ case. Lastly the scale parameter has been varied leading to the value $\sigma = 0.24$. It therefore seems that log-stable distribution are adequate to describe the mass distribution in this intermediate Weber number spray.

3. "Computing" the Mass Distribution

The goal of this section is to tentatively show how these two fitting parameters can be computed. Using equation (13), it can be seen that for the $We = 281$ case, the ratio λ_{EY}/D_0 equals 0.21 whose decimal logarithm is -0.67 close to the value used in the fit for the shift parameter δ. However, there is a stretch from comparing a wavelength and a final droplet size, so we will let this approximate result pending, for so far...

In order to compute the scale parameter, we have to consider that it sets the size of the "multiplier" in the cascade model and hints are that the first step should be governed by Entov & Yarin instability while the last step should be governed by Rayleigh-Taylor instability. The hint for this last assertion can be found on the scaling for the SMD/D_0 ratio of figure 6 is close to what can expected from Rayleigh-Taylor instability (*cf.* equation (23)). Let us review this more thoroughly: we consider a secondary droplet, whose diameter will be assumed to be D_1, and supersede its deceleration $f = dU_r/dt$ (where U_r is the relative velocity between the droplet and the surrounding fluid) to the gravity acceleration g in equation (10), using the classical approximation

$$\frac{\pi D_1^3}{6}\rho_L\frac{dU_r}{dt} = -\rho_C y^2 \frac{\pi D_1^2}{4} C_d U_r^2 \tag{20}$$

where y is the droplet extension due to its deformation by the flow (*cf.* [29] for instance) which yields

$$f \approx \frac{3}{2}\frac{\rho_C}{\rho_L}\frac{y^2}{D_1}C_d U_0^2 \tag{21}$$

assuming $U_r \approx U_0$. We then get

$$\frac{\lambda_{RT}}{D_1} \approx \pi\frac{1}{y}\sqrt{\frac{16\gamma}{C_d\rho_C U_0^2 D_1}} \tag{22}$$

or

$$\frac{\lambda_{RT}}{D_1} \approx \pi\frac{1}{y}\sqrt{\frac{8}{C_d We_{D_1}}} \tag{23}$$

Now assume that $D_1 \approx \lambda_{EY}$, this leads to

$$\frac{\lambda_{RT}}{\lambda_{EY}} \approx \frac{\pi}{y}\sqrt{\frac{8}{C_d We_{\lambda_{EY}}}} = \frac{\pi}{y}\sqrt{\frac{8}{C_d We}}\sqrt{\frac{D_0}{\lambda_{EY}}} \tag{24}$$

Note that it is an important step in this "cascade" modeling: instead of computing the wavelength of Rayleigh-Taylor instability on the jet diameter, it has been chosen to use the Entov & Yarin primary instability wavelength, thereby generating a (simplified) instability cascade mechanism. Assuming $y = 2$ and $C_d = 1.3$ (like in [20] except that here the drag coefficient of a flat plate is used), this leads for the $We = 281$ case to

$$\frac{\lambda_{RT}}{\lambda_{EY}} \approx 0.55 \tag{25}$$

Now we make the hypothesis that the size of the step is given by

$$\sigma = Log_{10}(\frac{\lambda_{RT}}{\lambda_{EY}}) \approx -0.25 \tag{26}$$

and the result is close to the value obtained by fitting the width of the distribution. Note that idea of relating some parameters of the self-similar fragmentation equation to the ratio of instability wavelengths, seen has the first step of the "cascade", has been previously attempted by Gorokhovski *et al.* [30] taking inspiration from the work of Varga *et al.* [31]. It concerned only Kelvin-Helmholtz and Rayleigh-Taylor instability however (which we attempted here without success).

We can try, now, to improve our estimate of the shift parameter δ. First, we can assume that the droplet size D_1 obtained from the Entov-Yarin step should be given by

$$\frac{\pi D_0^2 \lambda_{EY}}{4} = \frac{\pi D_1^3}{6} \tag{27}$$

assuming volume conservation between an unstable cylinder and a daughter spherical droplet, which leads to

$$\frac{D_1}{D_0} = \sqrt[3]{\frac{3}{2}\frac{\lambda_{EY}}{D_0}} \approx 0.68 \tag{28}$$

Then assuming bag breakup in the Rayleigh-Taylor step, it can be assumed that first, 75% of the droplet volume goes into the ring droplets [20], once rearranged, these droplets are half the size of the initial ring volume (generating around 8 main daughters on the average), so

$$\frac{D_2}{D_1} \approx \frac{1}{2}\left(\frac{3}{4}\right)^{\frac{1}{3}} \approx 0.45 \tag{29}$$

Therefore the shift parameter can be assumed to be

$$\delta = Log_{10}(\frac{D_2}{D_0}) \approx -0.51 \tag{30}$$

closer to the value obtained by fitting the PDF than our initial guess.

To conclude this part, it seems that the log-stable Mass PDF that has been found as an asymptotics to the self-similar fragmentation is also valid in this two-step cascade model (Entov & Yarin and Rayleigh-Taylor). Actually the self-similar fragmentation equation is also known in chemical engineering as the homogeneous fragmentation equation (see [32] for instance) without resorting to self-similarity arguments. This may explain why, in this low Weber number case, the asymptotic result may still be valid whereas the "cascade" is actually quite short as two steps are only required and high-speed video footage do not show droplets breaking up again and again. Last, let us precise that it was not possible to use this model for the $We = 39$ case or lower as equation (24) leads to value greater than one for the ratio between Rayleigh-Taylor and Entov & Yarin wavelengths and there should be, therefore, no second step. Likely the $We = 225$ case gives value too close to the analyzed case to be of interest. Moreover, though this part is entitled "Computing" the distribution, either the value of y or C_d (or both) can be seen as fitting parameter(s) in the end (though the values used are in the appropriate range).

B. "Inverse Cascade" on Turbulent Length Scale

Though the smallest droplet does carry only a slight part of the whole mass of the spray, they are quite numerous. Moreover their size may be compatible with turbulent length scale computed on table IV.

The log-stable model developed in [20] is a re-agglomeration process of the ligaments driven by the turbulence generated in the carrier phase. As such it can also be seen as an "inverse cascade" model as it ultimately generates scale larger than smaller size of the initial ligaments. Result of this model is shown as a blue line on figure 10.

In this model, the scale and shift parameter of the Number log-stable PDF, σ_{lnd} and δ_{lnd}, can be computed from the turbulent length scales using first equation (31) and then equations (36) and (37). Equation (31) allows to compute the scale parameter $\sigma_{ln\epsilon}$ of the turbulence dissipation log-stable PDF.

$$\sigma^{\alpha}_{\ln \varepsilon} = \ln \frac{\lambda_T}{\eta} = 3.43, \tag{31}$$

where α still equals 1.7 and Taylor and Kolmogorov scales have been previously defined in eq. (15) and (16). Turbulence dissipation rate and length scales are estimated by eq. (32,33,34).

$$\varepsilon \cong \frac{u'^3}{L_{\text{int}}} \cong \frac{1^3}{1.10^{-3}} \cong 1000 m^2/s^3 \tag{32}$$

$$\lambda_T = \sqrt{20\nu\frac{1,5}{1000}} \simeq 173\mu m \tag{33}$$

$$\eta \cong \left(\frac{\nu^3}{\varepsilon}\right)^{1/4} \cong 5.6\mu m \tag{34}$$

Let us note that $Log_{10}(0.173) = -0.76$ while $Log_{10}(0.0056) = -2.255$. These values correspond respectively to the mode and the low end of the blue PDF depicted on figure 10. Also note that the Kelvin-Helmholtz wavelength and other instability related wavelengths are not in the PDA measurement range as, for instance:

$$\lambda_{KH} = 3\pi \frac{0.41\,(1000 + 7994)}{2.5^2 \times 1000 \times 7994} \approx 695\mu\text{m} \qquad (35)$$

and $Log_{10}(0.695) = -0.15$.

The shift and scale parameter of the distribution can be computed using

$$\delta_{\ln d} = Log_{10}\left(\frac{\lambda_T}{D_0}\right) = -0.76 \qquad (36)$$

$$\sigma_{\ln d} = \frac{1}{2}\sigma_{\ln \varepsilon} = \frac{1}{2}(3,43)^{\frac{1}{1.7}} \approx 1.0 \qquad (37)$$

Figure 10 shows the result of the superposition of Lévy stable laws with parameters $\alpha = 1.7$, $\beta = -1$, $\delta = \delta_{lnd}$, $\sigma = \sigma_{lnd}$. No fitting is made and only the vertical axis (i.e. the number of droplets obeying to the proposed law) is varied. More details of the model can be found in [20].

IV. CONCLUSION

In this work, it has been shown, by sieving solidified fragments, that for a moderately low Weber number spray, the mass distribution follows a log-stable law. These laws were introduced [11] as asymptotic solution to the self-similar fragmentation equation. This equation is usually believed to be a mathematical translation of the recurrent "cascade" models (stemming from Richardson's idealization of turbulence) whereas, in the present case, the cascade seems to be far from developed: no drops seems to divide more than once or twice on the video footage that we examined. Nevertheless, it seems possible to compute all the parameters of the distribution (or rather an approximation of their value) by considering a self-similar cascade of instability: the first step being given by Entov & Yarin bending instability and the second step being given by Rayleigh-Taylor instability. This is valid however only for the large scales (*i.e.* droplet size) that contains most of the initial mass. These scale are much larger than the characteristic turbulent length scale of the jet.

To look at the small scale sensitive to turbulent agitation, we had to slow down the jet and use a phase Doppler anemometer. The resulting Number PDF still seems to follow a log-stable law but only from the Taylor scale to the Kolmogorov scale. The process at works being a process of turbulent re-agglomeration of the smallest ligaments, it has been described as an "inverse cascade". Note that, in the present case, while it concerns a huge number of small droplet, their mass is completely negligible.

It therefore seems that turbulent atomization seems to be a competition between several processes. This may explain the lack of universality observed in this field of study as the process may vary from one spray system to another (it is quite likely that air-blast atomizers are more sensitive to Kelvin-Helmholtz like instability than to Entov & Yarin bending instability for instance, or that swirl should have an impact...*etc.*). Moreover, it seems that, in present study, we have been lucky to observe sufficient scale separation between these effects; but this may not always be the case.

Lastly, due to the limited number of experiments and the difference in the experimental methods used (sieving *vs.* phase Doppler velocimetry), it has not been possible to precisely measure the competition (*i.e.* the mass ratio) between the "direct" and the "inverse" cascade to determine, experimentally, for instance, predominance regimes. This will need however a whole new (and larger) experimental setup (currently under development) that will allow to reach higher Weber numbers while maintaining converged statistics.

V. DECLARATION OF INTERESTS

The authors report no conflict of interest.

VI. ACKNOWLEDGEMENTS

The work was done under the research program on nuclear safety and radioprotection (RSNR) and received funding from French government managed by the National Research Agency (ANR) under Future Investments Program (PIA), research grant No: ANR-10-RSNR-01.

The authors also acknowledge partial support from COST action MP1305 "Flowing Matter", supported by COST (European Cooperation in Science and Technology).

[1] M. Pilch and C. Erdman, International Journal of Multiphase Flow **13**, 741 (1987).
[2] B. Gelfand, Progress in energy and combustion science **22**, 201 (1996).
[3] S. Saito, Y. Abe, and K. Koyama, Nuclear Engineering and Design **315**, 128 (2017).
[4] Y. Iwasawa and Y. Abe, Progress in Nuclear Energy **108**, 188 (2018).
[5] M. Hadj-Achour, N. Rimbert, M. Gradeck, and R. Meignen, The Physics of fluids **33**, 103315 (2021).

[6] E. Villermaux, P. Marmottant, and J. Duplat, Phys. Rev. Lett. **92**, 074501 (2004).

[7] N. Dombrowski and W. Johns, Chemical Engineering Science **18**, 203 (1963).

[8] A. N. Kolmogorov, in *Doklady of the Akademy of Sciences of the USSR*, Vol. 31 (1941) pp. 99–101.

[9] E. Novikov and D. Dommermuth, Physical Review E **56**, 5479 (1997).

[10] M. Gorokhovski and V. Saveliev, Physics of Fluids **15**, 184 (2003).

[11] N. Rimbert and O. Séro-Guillaume, Physical Review E **69**, 056316 (2004).

[12] R. Vallon, M. Abid, and F. Anselmet, Physical Review Fluids **6**, 023604 (2021).

[13] J. C. Beale and R. D. Reitz, Atomization and sprays **9** (1999).

[14] J. Eggers and E. Villermaux, Reports on progress in physics **71**, 036601 (2008).

[15] B. B. Mandelbrot, Nature , 394 (1982).

[16] D. Schertzer and S. Lovejoy, Journal of Geophysical Research: Atmospheres **92**, 9693 (1987).

[17] S. Kida, Journal of the Physical Society of Japan **60**, 5 (1991).

[18] N. Rimbert and O. Séro-Guillaume, Comptes Rendus Mécanique **331**, 775 (2003).

[19] N. Rimbert, Physical Review E **81**, 056315 (2010).

[20] N. Rimbert and G. Castanet, Physical review. E, Statistical, nonlinear, and soft matter physics **84**, 016318 (2011).

[21] V. Entov and A. Yarin, Journal of Fluid Mechanics **140**, 91 (1984).

[22] A. Amirzadeh, M. Raessi, and S. Chandra, Experimental thermal and fluid science **47**, 26 (2013).

[23] S. Chandrasekhar, *Hydrodynamic and hydromagnetic stability* (Courier Corporation, 2013).

[24] A. M. Sterling and C. Sleicher, Journal of Fluid Mechanics **68**, 477 (1975).

[25] S. Lin and D. Kang, The Physics of fluids **30**, 2000 (1987).

[26] R. D. Reitz, Atomisation Spray Technology **3**, 309 (1987).

[27] H. Tennekes and J. L. Lumley, *A First Course in Turbulence* (MIT Press, 1972) p. 300.

[28] G. Samorodnitsky and M. Taqqu, *Non-Gaussian Stable Processes: Stochastic Models with Infinite Variance*, edited by L. Chapman ft Hall (1994).

[29] N. Rimbert, S. C. Escobar, R. Meignen, M. Hadj-Achour, and M. Gradeck, Journal of Fluid Mechanics **904** (2020).

[30] M. Gorokhovski, J. Jouanguy, and A. Chtab-Desportes, Fluid dynamics research **41**, 035509 (2009).

[31] C. M. Varga, J. C. Lasheras, and E. J. Hopfinger, Journal of Fluid Mechanics **497**, 405 (2003).

[32] M. Kostoglou, Physica A: Statistical Mechanics and its Applications **320**, 84 (2003).